ACS APPLIED MATERIALS & INTERFACES

Article

Universal Method for Creating Hierarchical Wrinkles on Thin-Film Surfaces

Woo-Bin Jung, Kyeong Min Cho, Won-Kyu Lee, Teri W. Odom, and Hee-Tae Jung

ACS Appl. Mater. Interfaces, **Just Accepted Manuscript** • DOI: 10.1021/acsami.7b14011 • Publication Date (Web): 27 Nov 2017

Just Accepted

ACS Publications

ACS Applied Materials & Interfaces is published by the American Chemical Society.
1155 Sixteenth Street N.W., Washington, DC 20036

Universal Method for Creating Hierarchical Wrinkles on Thin-Film Surfaces

*Woo-Bin Jung[1,3], Kyeong Min Cho[1], Won-Kyu Lee[2], Teri W. Odom[2, 3], and Hee-Tae Jung[1,] **

[1]National Laboratory for Organic Opto-Electronic Materials, Department of Chemical and Biomolecular Engineering (BK-21 plus), Korea Advanced Institute of Science and Technology, Daejeon 305-701, South Korea

[2]Department of Materials Science and Engineering, Northwestern University, Evanston, Illinois 60208, United States

[3]Department of chemistry, Northwestern University, Evanston, Illinois 60208, United States

Corresponding authors

*E-mail: heetae@kaist.ac.kr

Keywords: Transition metal dichalcogenides, molybdenum disulfide, wrinkle, hydrogen evolution reaction, hierarchical wrinkles

Abstract

One of the most interesting topics in physical science and materials science is the creation of complex wrinkled structures on thin-film surfaces because of their several advantages of high surface area, localized strain, and stress tolerance. In this study, a significant step was taken toward solving limitations imposed by the fabrication of previous artificial wrinkles. A universal method for preparing hierarchical three-dimensional wrinkle structures of thin films on a multiple scale (e.g., nanometers to micrometers) by sequential wrinkling with different skin layers was developed. Notably, this method was not limited to specific materials, and it was applicable to fabricating hierarchical wrinkles on all of the thin-film surfaces tested thus far, including those of metals, two-dimensional and one-dimensional materials, and polymers. The hierarchical wrinkles with multi-scale structures were prepared by sequential wrinkling, in which a sacrificial layer was used as the additional skin layer between sequences. For example, a hierarchical MoS_2 wrinkle exhibited highly enhanced catalytic behavior because of the superaerophobicity and effective surface area, which are related to topological effects. As the developed method can be adopted to a majority of thin films, it is thought to be a universal method for enhancing the physical properties of various materials.

Introduction

Transformation of 2D surface into wrinkled 3D topologies is one of the most interesting issues in materials and nanotechnology researches, because of many advantages including high surface area, localized strain and stress tolerance.[1-3] This has been applied to a variety of fields including flexible hydrophobic surface, cell guiding, LC alignment, Li-ion batteries and supercapacitors.[4-8] In fact, there are a number of examples in nature such as fingerprint[9], wrinkled cell membrane[10] and skins of plant and fruits, which is generated from deformation mismatch in skin and substrate layered structures. On the other hand, winkle structure of common organic and inorganic materials is prepared by mechanical instability between 2D layers and stress resistances of each layer. When substrates are stretchable or shrinkable, various materials including metal, polymer, graphene, graphene oxide films can be wrinkle structures on the substrates by releasing strain or shrinking with heating.

The creation of complex and tunable wrinkle structures is one of the most important issues in physical science and materials science because of their advantages of high surface area and localized strain. Many researchers reported complex and tunable wrinkle including hierarchical wrinkling.[11-14] In particular, hierarchical wrinkle, multiple wrinkle with different feature size in a single system, is important because of very high surface area and its superior wettability.[11, 15-18] However, existing methods for the formation of hierarchical wrinkles are complicated and have limitations in types of materials and feature dimensions. In other words, each method can be adopted to only certain types of materials. For examples, gold wrinkle structure on buckling was generated by high strain relief.[19] In the range of higher strain over the range of wrinkle generation, buckling is generated with larger wavelength containing several number of wrinkles. Hierarchical wrinkles of polymer film such as polypyrrole or fluoric polymer were generated by

sequential wrinkling with growth of polymer[20-21]. In case of graphene oxide, hierarchical wrinkle can be achieved by multiple transfer and shrinking processes.[15] In additions, almost hierarchical wrinkle system, excepting polymer growth method, cannot independently control feature dimensions of hierarchical wrinkle because larger wavelength is determined by thickness of materials.

In here, we developed a universal method for forming hierarchical wrinkles on materials such as metals, polymers, graphitic carbon materials, and other two-dimensional (2D) materials with high controllability. Very importantly, this method is not limited to specific materials, and can be employed for fabricating hierarchical winkle of all thin films that we tested thus far. Our technique simply uses a sacrificial layer such as a polyvinylpyrrolidone (PVP) layer onto wrinkle of target materials, which acts as a skin layer for forming larger wavelength. Multiple hierarchical wrinkle over 3 can be fabricated by just repeating hierarchical wrinkling method. Through our method, we simply and independently controlled each wavelength of first (G1) and second (G2) generations of wrinkles. We found that a critical concentration of PVP for the formation of hierarchical wrinkles exists. We found that the resulting hierarchical MoS_2 wrinkle showed highly enhanced catalytic behavior due to high effective surface area and superaerophobicity from topological effect. Because of universality, we believe that this technique can be universal method for bottom-up texturing of various materials.

Result and Discussion

Figure 1a shows the overall fabrication process for hierarchical wrinkle structures on thin-film surfaces. First, various thin films, namely, metals, two-dimensional (2D) materials (e.g.,

graphene, MoS_2, WS_2, and SnS_2), one-dimensional (1D) materials (e.g., carbon nanotubes), and polymer films, with different thicknesses (h_1) were coated onto a pre-strained polystyrene (PS, glass transition temperature (T_g) = 120 °C) film by appropriate methods, depending on the types of target materials. The thin-film wrinkles on the PS substrate were generated by heating at a temperature above the glass transition temperature (i.e., ~120 °C) in the oven (~135 °C) and cooling to room temperature[22-25]. The areal strain (ε, $\varepsilon = (A_0 - A_f)/A_0$), where A_0 and A_f respectively denote the areas before and after strain relief, was controlled by simply changing the heating time in the oven. To generate the second wrinkle (G2) at a larger wavelength, a sacrificial skin layer (thickness ≈ h_2) was coated onto the first wrinkle film (G1). By the same strain-relief process, G2 was generated at a larger wavelength with keeping morphology of G1. After fabrication of the hierarchical wrinkles, the sacrificial skin layer was rinsed using suitable solvents; here, the solvents do not change the structure, morphology, and feature dimension of the wrinkled thin film. In this study, polyvinylpyrrolidone (PVP, M_w = 360,000 g/mol, T_g = 150 °C) was mainly used as the sacrificial skin layer because it could be easily removed using ethanol[26] without any damage to the first skin layer. After the removal of the PVP skin layer by simply rinsing with ethanol, G1 and G2 wrinkles were exposed. Interestingly, a wrinkle generation over the second generation (G2) was obtained by repeating the hierarchical wrinkling cycle through strain relief after coating a sacrificial layer at each cycle. After n cycles, multiscale wrinkles from G1 to G(n+1) with the largest wavelength ($\lambda_{G(n+1)}$) were obtained. Notably, this extremely simple approach can be applied to mass production because only sacrificial skin layers are required to fabricate hierarchical wrinkles without any additional transfer and complicated processes.

Figure 1b shows the scanning electron microscopy (SEM) images of a representative MoS_2 hierarchical wrinkle with a multiscale structure after four hierarchical wrinkling cycles. A few-layered MoS_2 film ($h_1 \approx 9.8$ nm) on a SiO_2/Si wafer was prepared by chemical vapor deposition (CVD)[27] and then identified by its Raman spectrum (**Figure S1**). The MoS_2 film was then transferred onto the PS substrate by a Poly(methyl-methacrylate) (PMMA)-assisted transfer method[28]. After the first strain-relief process by heating above the glass transition temperature (120 °C), the first-generation wrinkle (G1) was formed on the PS film. The PVP coating (concentration of PVP (C_{PVP}) = 0.5 wt%), which was followed by a second strain-relief process, generated the second-generation (G2) wrinkle on the G1 wrinkle film over the entire surface. Repeating the four cycles of hierarchical wrinkling process produced the fifth generation of hierarchical wrinkles, and higher generation is also possible if we repeat more hierarchical wrinkling process.

At above the T_g, the MoS_2-PS film shrunk during thermal heating, leading to $\varepsilon = 0.30$ at each cycle ($\varepsilon_{total} = 0.84$). The feature dimension of the wrinkles was determined from the average measurement of SEM and AFM images with using image processing program. Careful inspection of the SEM images clearly revealed wrinkles with a large wavelength (wavelength of G5 (λ_{G5}) $\approx$ 200 μm, red line of the top-left inset image; $\lambda_{G4} \approx 20$ μm, green line of **Fig. 1b**), and a high population of wrinkles with shorter wavelength ($\lambda_{G3} \approx 6$ μm, blue line in the inset images) present in the long-wavelength wrinkles. At high magnification, $\lambda_{G2} \approx 1$ μm and $\lambda_{G1} \approx 330$ nm were clearly apparent.

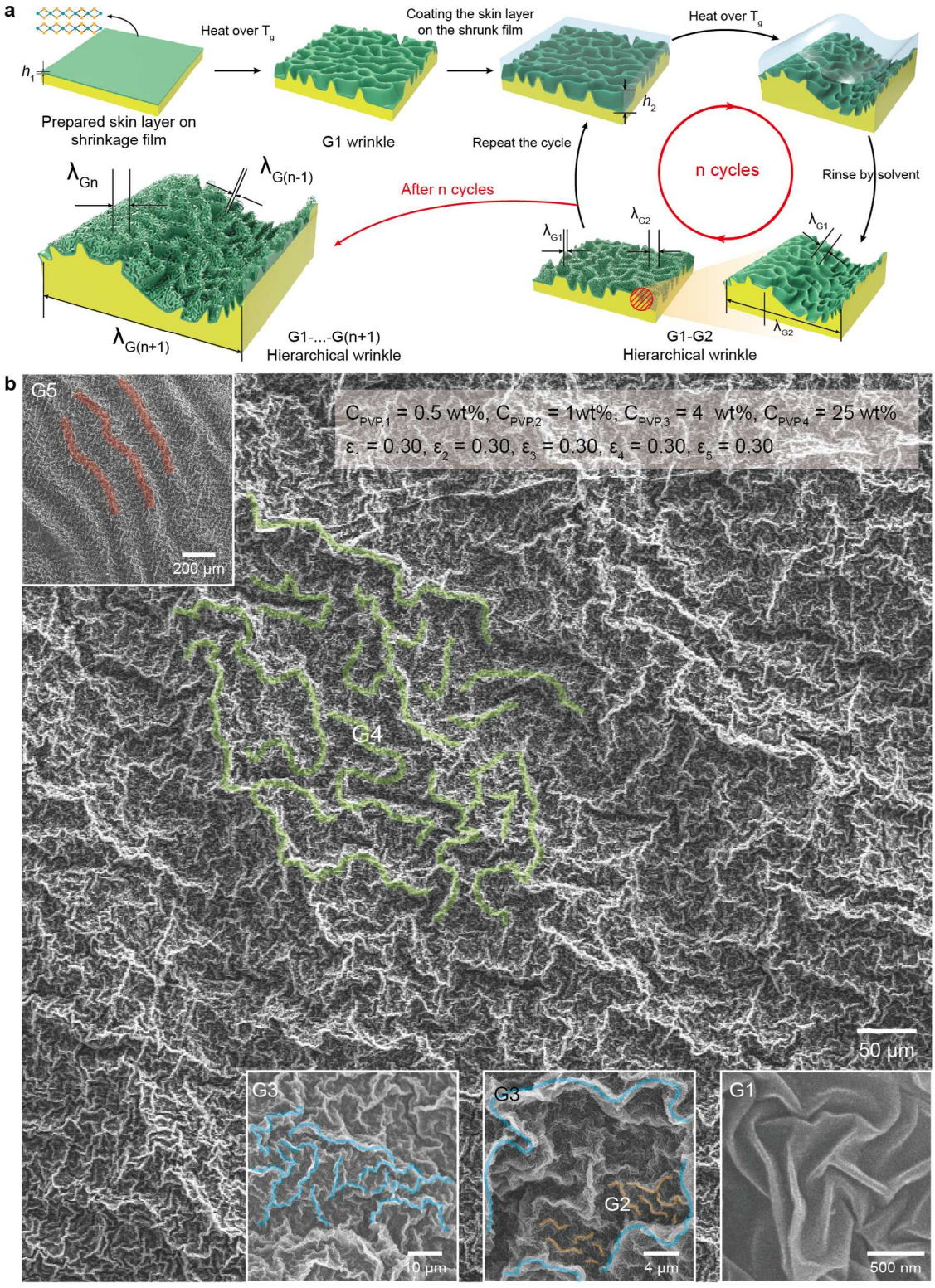

Figure 1. Schematic for the fabrication of hierarchical wrinkles. (a) Hierarchical wrinkling process **(b)** Hierarchical MoS_2 wrinkle including G1–G5 after four cycles of hierarchical wrinkling.

Surprisingly, this approach for fabricating hierarchical wrinkles is not limited to the MoS_2 film. This method can be applied to a majority of thin-film materials from metals to polymers, including gold, 2D materials (e.g., graphene derivatives, MoS_2, WS_2, and SnS_2), 1D carbon nanotubes, polyolefin (PO) and PS films (**Figure 2**). A hierarchical gold wrinkle film (**Figure 2a**) was prepared after one cycle of the hierarchical wrinkling of a gold film that was deposited by an e-beam evaporator. λ_{G1} of a 25 nm thick gold film was ~500 nm after the first strain relief (ε = 0.30); here, λ_{G1} was greater than that of polymers because of the thicker film and the higher Young's modulus of gold[29]. After the spin-coating of a 5 wt% PVP solution on the first gold wrinkle film, followed by thermal heating, the PVP-coated Au wrinkle film decreased to ε_{total} = 0.60, resulting in a λ_{G2} of ~8 μm.

In addition, this method can be applied to the generation of hierarchical wrinkles of various 2D materials, such as graphitic carbon materials (**Figure 2b** and **2c**) and transition metal dichalcogenides (**Figure 2d–2f**). CVD-grown[30] monolayer graphene (**Figure S2**) exhibited a wrinkle with the smallest λ_{G1} of ~36 nm because of extremely low film thickness (~1 nm; Fig. 2b)[31-32]. Graphene oxide (GO) exhibited a relatively high λ_{G1} compared with CVD graphene (Fig. 2c) because of the thicker film[33-34]. Despite spin-coating of the PVP solution (1 wt%) onto CVD-grown graphene and GO G1 wrinkles to generate hierarchical wrinkles, the λ_{G2} of GO (~8 μm) was greater than that of CVD graphene (~1 μm).

Figure 2d– 2f shows the hierarchical wrinkles of other 2D materials, including WS_2, SnS_2, and 1T-MoS_2. WS_2 and SnS_2 synthesized by CVD[35-36] produced typical Raman shifts (**Figure S3**). Hierarchical WS_2 and SnS_2 wrinkles exhibited higher λ_{G1} (~180 nm and ~140 nm) and λ_{G2} (~2 μm and ~1.6 μm) values compared with graphene. Unlike CVD-grown materials, 1T-MoS_2 was synthesized by a hydrothermal method in an autoclave[37]. Because of the different

synthetic method, sheet-like 1T-MoS_2 (inset image in Fig. 2f) with different chemical properties was obtained (**Figure S4**). 1T-MoS_2 dispersed in water was spin-coated onto PS as a thin film, and the resulting composite was subjected to the hierarchical wrinkling process. Because of its high film thickness, λ_{G1} (~1.6 μm) and λ_{G2} (~11 μm) were greater than those of other 2D materials.

Figure 2g shows the hierarchical wrinkles obtained by using 1D carbon nanotube (CNT) materials. To fabricate CNT wrinkles, CNT (0.2 mg/ml) dispersed in surfactant solutions[38] was spin-coated onto the PS film. The inset in the top left SEM image of **Figure 2g** shows the CNT network film. After the hierarchical wrinkling process, hierarchical CNT wrinkles with $\lambda_{G1} \approx$ 1.6 μm and $\lambda_{G2} \approx 15$ μm were observed.

This developed method can be applied to a majority of the polymer thin films. **Figure 2h** and **2i** shows the hierarchical wrinkles of freestanding polyolefin (PO)[39] and PS films. In this case, the PVP solution (C_{PVP} = 0.5 wt%) was spin-coated onto each film as the first skin layer. After relieving of the strain and rinsing off of PVP using ethanol, G1 wrinkles remained on the monolithic PS and PO films. The λ_{G1} values of PO and PS were ~54 nm and ~180 nm, respectively. For the hierarchical wrinkles, 2 wt% PVP was spin-coated again and subjected to the hierarchical wrinkling process. Finally, monolithic, hierarchical PO and PS wrinkles with λ_{G2} of ~1.2 μm for PO and ~3.6 μm for PS were obtained.

Accordingly, this developed approach could be used to fabricate hierarchical wrinkles of a majority of the thin films if the hierarchical wrinkling process satisfied three conditions: (1) Substrates (PS in this study) are not damaged during the deposition of target materials on the substrate. (2) During the deposition and rinsing of sacrificial skin layers (PVP in this study), the structure, morphology, and feature dimensions of the first skin layer and substrate should not be

changed. (3) λ_{G2} should be greater than the critical conditions ($\lambda_{G2,\,cr}$) to allow formation of hierarchical wrinkles and to be proportional to λ_{G1}.

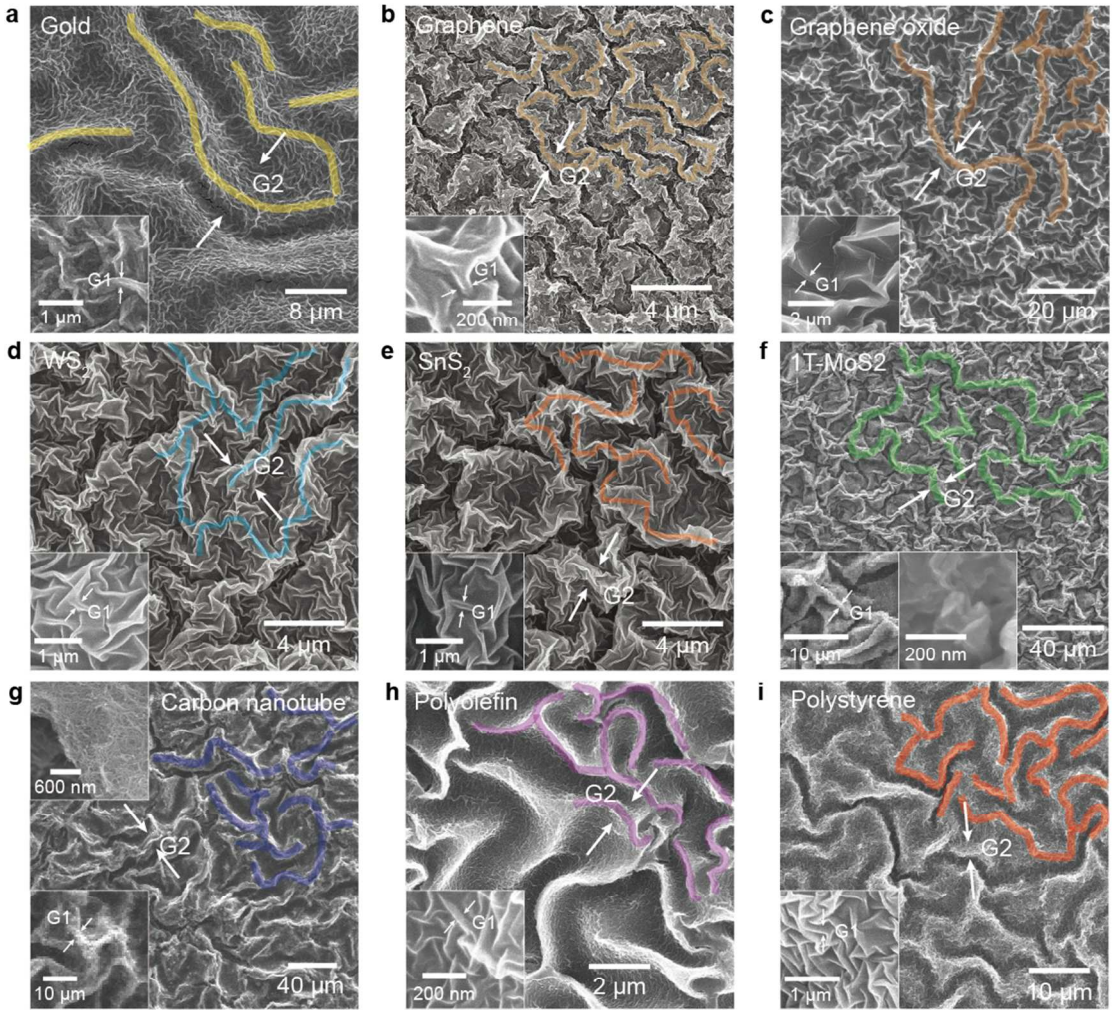

Figure 2. Hierarchical wrinkles obtained by using various materials. (a) Gold, **(b)** Graphene, **(c)** graphene oxide**, (d)** tungsten disulfide (WS_2), **(e)** tin disulfide (SnS_2), **(f)** 1T-MoS_2, **(g)** carbon nanotubes, **(h)** polyolefin, and **(i)** polystyrene. Inset images show high-magnification SEM images002E

The feature dimensions of the wrinkles could be controlled by tuning the thickness (h_1) of the target materials. The wrinkles of a bilayer system result from the instability between layers, and

the wavelength (λ) is proportional to the skin layer thickness[40], $\lambda = 2\pi h(\bar{E}_s/3\bar{E}_b)$ ($\bar{E} = E/(1-\nu^2)$), where E_s and E_b are the moduli of the skin layer and bulk substrate, respectively. **Figure 3a** shows λ_{G1} for MoS_2 films of different thicknesses. For example, h_1 of MoS_2 was controlled in the range from 9.8 nm to 46.3 nm, in which different h_1 values of MoS_2 were obtained by changing the Mo thickness during CVD, in order to tune λ_{G1} of MoS_2[27]. λ_{G1} linearly increased with the increase in h_1 of MoS_2; here, h_1 of MoS_2 was measured by atomic force microscopy (**Figure S6**): λ_{G1} ≈330 nm, λ_{G1} ≈ 870 nm, and λ_{G1} ≈ 1.30 μm MoS_2 with thicknesses of 9.8 nm, 25 nm, 46.3 nm respectively, at a fixed strain (ε = 0.3). Similar to λ_{G1} observed for MoS_2 thin films, that of graphene was tuned by changing the number of layers (**Figure 3b**), in which the number of graphene layers was controlled by repeating the transfer process. The λ_{G1} of graphene on the PS film linearly increased from 36 nm to 104 nm with the increase in the number of graphene layers from 1 to 4. Therefore, λ_{G1} is tunable by the simple control of the target material thickness (h_1).

Meanwhile, λ_{G2} could be controlled by tuning the thickness of the sacrificial PVP skin layer (h_2) and target materials (h_1). **Figure 3c** shows the SEM images of hierarchical MoS_2 wrinkles with tuned λ_{G2} of different PVP h_2 values, which was controlled by PVP concentrations (C_{PVP}). In here, we controlled C_{PVP} as a variable because coated PVP on wrinkled surface is affected by the roughness and types of materials. (**Figure S8**) PVP skin layers with different C_{PVP} values were spin-coated onto the G1 wrinkle (λ_{G1} = 333 nm for a 9.8 nm thick MoS_2). To isolate the effect of C_{PVP} on λ_{G2}, each strain was fixed at ε_{total} = 0.60 (ε_1 = 0.30 and ε_2 = 0.43 for G1 and G2, respectively). At C_{PVP} = 0.1 wt%, we observed, hierarchical wrinkles with a shape similar to that of the G1 wrinkle, except that it only had a higher λ_{G2}. With increasing C_{PVP}, λ_{G1} also increased, and the number of wrinkles decreased in the same area.

Figure 3d shows the λ_{G2} for different C_{PVP} values of MoS_2 and graphene. λ_{G2} linearly increased with the C_{PVP} for MoS_2, indicating that λ_{G2} of a 9.8 nm thick MoS_2 changes from 2.3 μm to 7.3 μm upon tuning of C_{PVP} from 0.05 wt% to 10 wt% (**Figure S9**). Such an increase was also observed for graphene (**Figure S10**). λ_{G2} of graphene increased from 320 nm to 6.5 μm with the increase in C_{PVP} from 0.1 wt% to 10 wt%.

In addition, λ_{G2} was significantly affected by the h_1 of target materials. The λ_{G2} values of MoS_2 with different thicknesses (h_1 = 9.8 nm, 15.8 nm, 25 nm, 38.3 nm) at a constant C_{PVP} (5 wt%) were compared (**Figures 3d** and **S11**). λ_{G2} increased from 5.9 μm (9.8 nm thick MoS_2) to 8.2 μm (38.3 nm thick MoS_2). Thus, thicker target materials lead to increased λ_{G1} and λ_{G2}. However, the possibility that λ_{G2} is affected by λ_{G1} cannot be ruled out. To prove it, λ_{G2} for two values of λ_{G1} at a fixed h_1 (20 nm) was investigated. To prepare G1 wrinkles with different λ_{G1} values at a constant h_1 (20 nm), a PVP sacrificial layer (1 wt%) was coated onto a 20 nm thick gold film, followed by rinsing after strain relief. The resulting G1 wrinkle exhibited a λ_{G1} of ~910 nm for a 20 nm thick gold film, while the gold wrinkle without PVP coating exhibited a λ_{G1} of ~430 nm (**Figure S12**). At C_{PVP} = 5 wt%, identical λ_{G2} values were obtained for two values of λ_{G1}: $\lambda_{G2} \approx 8.0$ μm at λ_{G1} = 430 nm and $\lambda_{G2} \approx 7.9$ μm at λ_{G1} = 910 nm. Similarly, at C_{PVP} = 7 and 10 wt%, constant λ_{G2} values were obtained at the same C_{PVP} for different λ_{G1} values, indicating that λ_{G2} is not affected by λ_{G1} (**Figure S13**). Hence, controlling h_1 changes λ_{G1}, and λ_{G2} is dependent on the equivalent thickness and Young's modulus of hybrid skin layer composed of h_1 and h_2 materials.

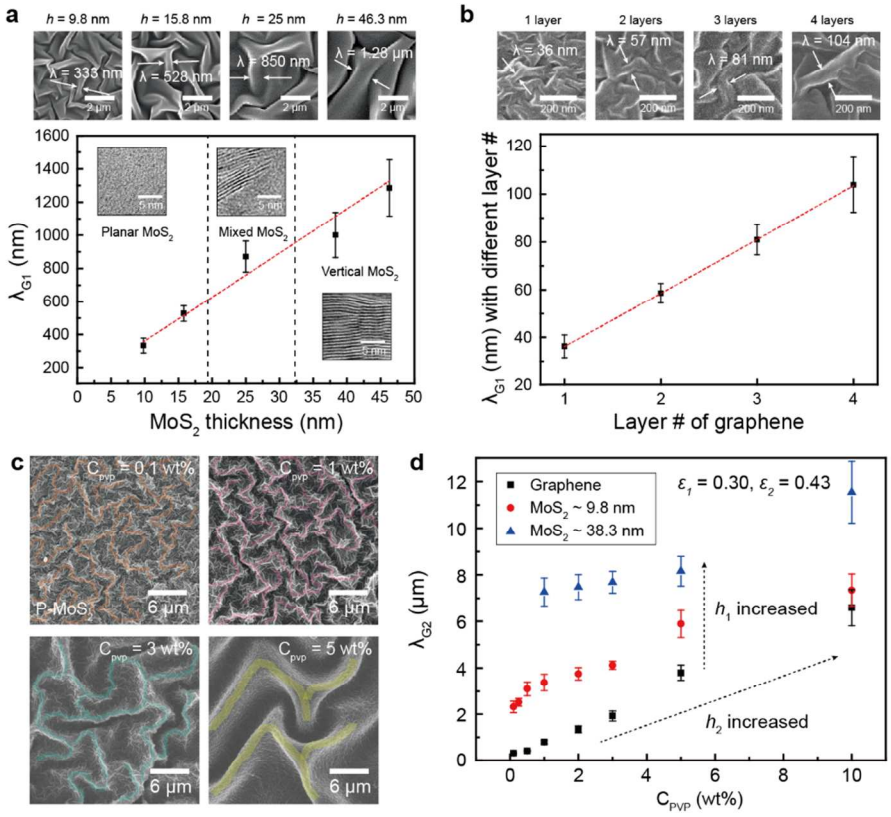

Figure 3. Tunable wavelength of hierarchical MoS_2 and graphene wrinkle. (a) Wavelength is proportional to the thickness of MoS_2, and each film exhibits different atomic structures. **(b)** Increase in the graphene layer for controlling λ_{G1}: **(c)** Hierarchical 9.8 nm thick MoS_2 wrinkle with different C_{PVP}, which changes λ_{G2}. **(d)** C_{PVP} versus λ_{G2}. λ_{G2} is proportional to C_{PVP} and skin thickness (h_1).

Interestingly, a critical C_{PVP} ($C_{PVP,\,cr}$) for the formation of hierarchical wrinkles exists. In other words, hierarchical wrinkles were formed above $C_{PVP,\,cr}$. For example, the formation of a G2 gold wrinkle on the G1 wrinkle (h_1 = 20 nm) started at a C_{PVP} of 0.25 wt%. $C_{PVP,\,cr}$ was found to be strongly dependent on λ_{G1}. To isolate the effect of λ_{G1}, h_1 was fixed at 20 nm, and only λ_{G1} was varied. **Figure 4a** shows the focused ion beam (FIB)-SEM images at various C_{PVP} values at two λ_{G1} (λ_{G1} of ~430 nm (top of **Fig. 4a**) and λ_{G1} of ~910 nm (bottom of **Fig. 4a**)) at a constant h_1 (20 nm). At a λ_{G1} of ~430 nm, the G2 wrinkle did not form at a C_{PVP} of 0.1 wt%,

revealing a more strained G1 wrinkle. The G2 wrinkle was observed at $C_{PVP, cr}$ = 0.25 wt% (top images of **Fig. 4a**), where small G1 wrinkles were included in the G2 wrinkles (red arrow). At $C_{PVP, cr}$ above 0.25 wt%, λ_{G2} of hierarchical wrinkle increased with C_{PVP}. Similarly, at a λ_{G1} of ~910 nm, the formation of the G2 wrinkle started at a $C_{PVP, cr}$ of 1 wt%. This concentration is greater than that at a λ_{G1} of 430 nm. Therefore, $C_{PVP, cr}$ increases with λ_{G1}, resulting in increased λ_{G2} at critical point ($\lambda_{G2, cr}$). **Figure 4b** shows the top-view images of hierarchical wrinkles at a $C_{PVP, cr}$ values of 0.25 wt% (top) and 1 wt% (bottom). λ_{G2} at a λ_{G1} of ~430 nm was ~2.6 μm, which increased to ~5.4 μm with the increase in λ_{G1} from 430 nm to 910 nm. Hence, $\lambda_{G2, cr}$ depends on λ_{G1}.

Figure 4c shows plots of λ_{G1} versus $\lambda_{G2, cr}$ of various materials, namely, MoS_2, graphene, and gold. Similar to the $C_{PVP, cr}$ values of gold (yellow), those of MoS_2 (red) and graphene (blue) were dependent on λ_{G1}. $\lambda_{G2, cr}$ of the materials almost linearly increased with λ_{G1}, which means that thicker sacrificial layer (PVP) is needed to generate G2 wrinkle on larger G1 wrinkle. We attributed to that G2 wrinkle is generated when G2 wavelength can include the several number of G1 wavelength. Hierarchical wrinkles formed within the upper range of critical conditions and were absent within the lower range. The $\lambda_{G2, cr}/\lambda_{G1}$ ratio was not considerably different among the materials; $\lambda_{G2, cr}/\lambda_{G1}$ ratio of gold, MoS_2, and graphene were ~6.0, ~7.1, and ~8.75, respectively (**Figure S18**). The slight increase in the $\lambda_{G2, cr}/\lambda_{G1}$ ratio is related to the different moduli, as it depends on the material (Young's modulus of gold (E_{gold}) ≈ 50 GPa, E_{MoS2} ≈ 200–300 GPa, $E_{graphene}$ ≈ 1000 GPa).

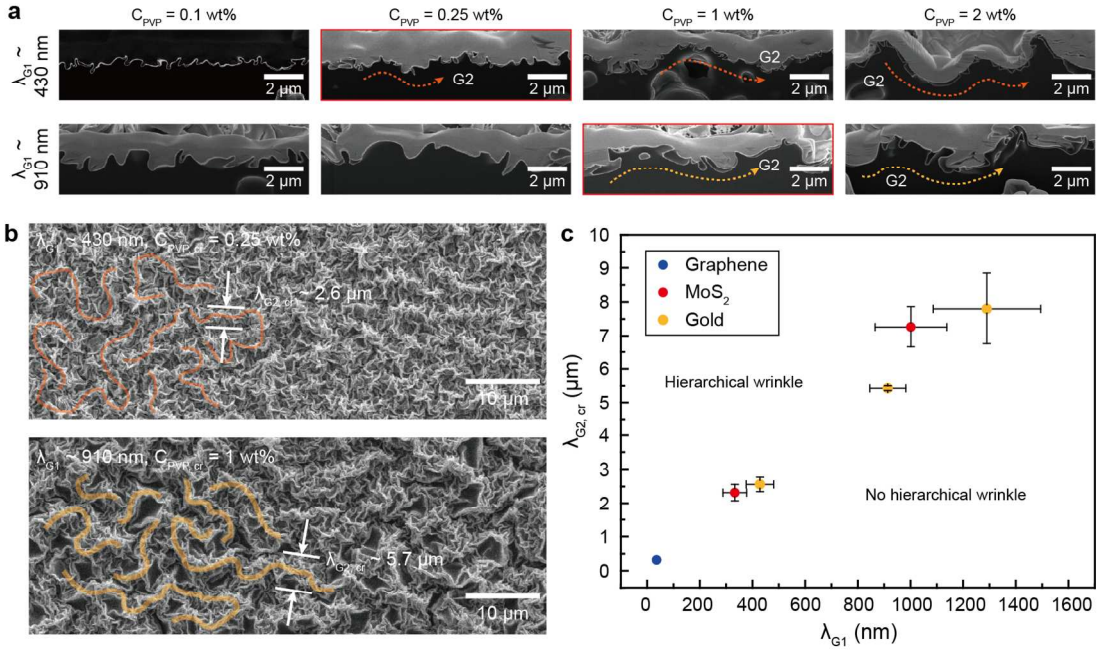

Figure 4. Critical conditions for the formation of hierarchical wrinkles. (a) FIB-SEM images of hierarchical Au wrinkles with λ_{G1} and C_{PVP} from 0.1 wt% to 2 wt%. **(b)** SEM images at $C_{PVP, cr}$. **(c)** λ_{G1} vs. $\lambda_{G2, cr}$ plots for the materials with MoS_2, graphene, and gold.

To demonstrate the novelty of the hierarchical wrinkle structure, the hierarchical MoS_2 wrinkles were compared against the primary wrinkles and flat MoS_2 by examining their activities in the hydrogen evolution reaction (HER). In recent years, MoS_2 has attracted considerable attention as alternative catalysts to platinum because of its high stability and catalytic activity[41-43]. For the HER tests, flat MoS_2 and MoS_2 wrinkles with primary and hierarchical shapes on the Au–PS substrate were fabricated (**Figures S19** and **S20**), where vertical aligned MoS_2 was utilized. The linear sweep voltammetry (LSV) curves of the MoS_2 wrinkle exhibited considerably enhanced performance with a lower overpotential compared with flat MoS_2 wrinkles. (**Figure 5a**) Among the primary wrinkles, the overpotential at 10 mV/cm^2 decreased from 473.7 mV to 272.6 mV with increasing strain from ε = 0.00 to ε = 0.78. Hierarchical wrinkles with an ε_{total} of 0.60 exhibited the best performance at an overpotential of 256.9 mV.

Figure S21 shows a plot of the overpotential at −10 mA/cm^2 versus strain for hierarchical MoS_2 wrinkles, which exhibited considerably more efficient wrinkling for the HER. Hierarchical wrinkles exhibited the lowest overpotential of 256.9 mV even though its ε_{total} of 0.60 was less than that of a single-generation wrinkle. Within the same strain on the primary and hierarchical wrinkles, hierarchical wrinkles exhibited a lower overpotential, indicating that hierarchical wrinkles are more efficient at increasing the catalytic performance. The corresponding Tafel plots show that the Tafel slope decreases because of the wrinkled structures (**Figure 5b**). The Tafel slope is a useful method for evaluating the rate-limiting mechanism of HER[44]. The Tafel slopes for the G1 wrinkle decreased from 134.5 mV/dec to 100.1 mV/dec, while those for the hierarchical wrinkle decreased to 72.6 mV/dec. Hierarchical MoS_2 wrinkles with a Tafel slope of 72.6 mV/dec were responsible for the Volmer–Heyrovsky HER mechanism. These higher Tafel slopes compared with that of Pt/C (~30 mV/dec)[45] are related to the low adsorption of hydrogen (H_{ads}) on the MoS_2 surfaces.

To evaluate the durability of the MoS_2 wrinkle, a hierarchical MoS_2 wrinkle catalyst was cycled at a scan rate of 100 mV/sec for 1000 cycles (**Figure S22**). After 1000 cycles, the catalyst exhibited similar electrocatalytic behavior as before, with only negligible loss of activity.

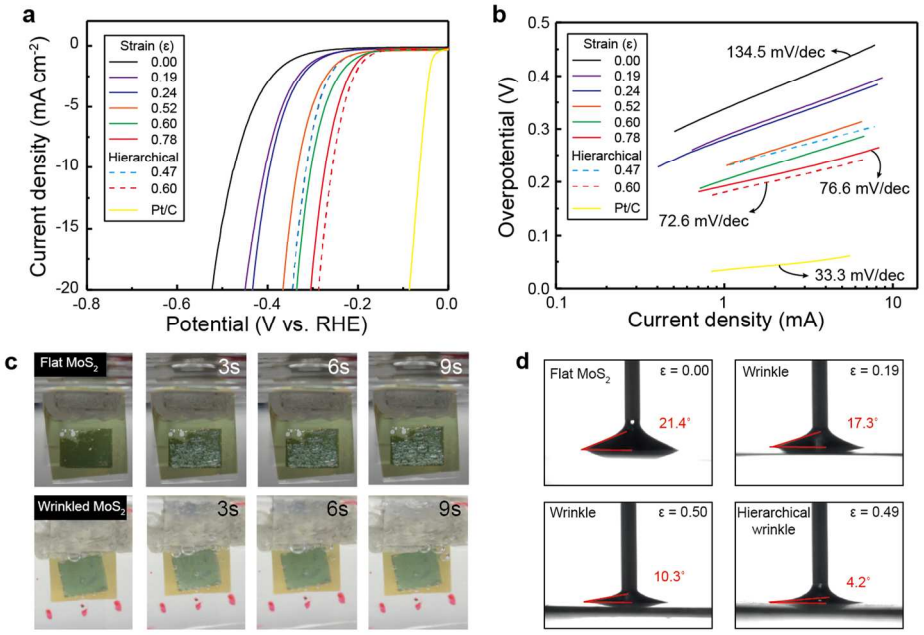

Figure 5. Effect of wrinkles on the HER activity of MoS_2. (a) LSV curves of primary wrinkles, hierarchical wrinkles (dashed line) at various strain values, and the Pt/C reference. **(b)** Corresponding Tafel plots of the LSV curves. **(c)** Photograph of the surfaces of flat and wrinkled MoS_2 surfaces producing hydrogen gas. **(d)** Receding contact angles on flat MoS_2 and on various wrinkles.

The enhanced HER catalytic performance of hierarchical MoS_2 wrinkles is related to the superaerophobic wettability. Superaerophobicity, which is repelling air such as gas bubble in liquid, on the primary and hierarchical MoS_2 wrinkles was expected[46-47]. To clearly understand and reveal the effect of wrinkle, the flat and wrinkled MoS_2 surfaces were observed during hydrogen gas production (**Figure 5c**). With the flat MoS_2 film, the hydrogen gas bubble strongly adhered to the surface and continuously enlarged until it detached. The increase and release of the large bubble led to fluctuations in the LSV curve and even decreased the working area of the catalyst (**Figure S23**). By contrast, the hydrogen bubble on the MoS_2 wrinkle did not adhere to the surface for a long time and rapidly detached before the size increased. To quantitatively compare the superaerophobicities, the receding angles were measured (**Figure 5d**). The receding

angle was related to the growth of gas bubbles in the aqueous electrolyte (**Figure S24**). On the surface with a low receding angle, the gas–surface contact area remained small, and the growing gas bubbles easily detached. The hierarchical MoS_2 wrinkle with an ε_{total} of 0.49 exhibited a receding angle of 4.2 °, which effectively blocked the dead space from the gas–surface contact area and produced fluctuations due to gas bubbles. The additional performance enhancement of the hierarchical wrinkle was obtained from the efficient maximization of the highly strained surface area. In the SEM and FIB-SEM images (**Figure S25**), the primary wrinkles at ε = 0.50 exhibited partially folded structures; the corresponding stacked MoS_2 surface did not function as a catalyst (**Figure S26**). By contrast, even though we observed almost the same strain (ε_{total} = 0.49) with the primary wrinkles (ε = 0.50) for the hierarchical structures, the hierarchical structure exhibited a completely open surface, including a low-strain wrinkle. Hierarchical wrinkling was thus the most effective method for the transformation of 2D materials to three-dimensional structures without the loss of the effective catalytic surface area.

Conclusion

In summary, a universal method for creating hierarchical wrinkles with various materials was developed. We formed hierarchical wrinkles using a sacrificial skin layer (PVP) on the previous wrinkle, with the PVP layer generating larger wrinkles during the second strain relief that were easily rinsed. Various materials (from metals to 2D materials and polymers) were used as hierarchical wrinkle materials. For hierarchical wrinkles, a critical $\lambda_{G2}/\lambda_{G1}$ ratio, which depended on the type of materials, existed. The MoS_2 wrinkles used in the HER exhibited enhanced performance in the reaction. This enhanced HER performance of the hierarchical wrinkles was related to the superaerophobicity and increase in effective surface area without surface loss. Hierarchical wrinkles exhibited potential advantages in their used in

superhydrophobic surfaces, photo- and electrocatalysts, and photonic devices, e.g., photoelectron chemical catalysts, photodetectors, and devices for surface-enhanced Raman spectroscopy applications. Especially, multi generation of wrinkles can be advantageous to get larger surface area in catalysis compared to singular wrinkle and to show superior wetting behavior.

Experimental section

Preparation of MoS_2. MoS_2 films with different atomic structures with different thicknesses of Mo were synthesized by chemical vapor deposition (CVD). Mo was deposited on a SiO_2/Si wafer by e-beam evaporation. Mo films were loaded in the furnace for sulfurization. Sulfur (purchased from Sigma-Aldrich) was loaded in the heating zone at 200 °C, which was before the Mo film heating zone (770 °C). The quartz tube was evacuated to 50 mTorr and then purged with argon (Ar) at 50 sccm for 30 min. For the heating process to grow MoS_2, Mo films were heated to 770 °C for 30 min and maintained at this temperature for 15 min. After the growth of MoS_2, the furnace tube was rapidly cooled to room temperature. The final MoS_2 atomic structures depended on the Mo thickness: planar MoS_2 from 2 and 5 nm thicknesses; mixed MoS_2 from 10 nm thicknesses; and vertical MoS_2 from 15 and 20 nm thicknesses (**Figure S6**).

Preparation of graphene. The Cu foil (25 μm thickness; Goodfellow, 99.99%) was placed in a quartz tube, which was then heated to 1040 °C under H_2 at 8 sccm. After annealing for 1 h, CH_4 at 50 sccm was then injected into the furnace along with H_2 for 15 min. The film was rapidly cooled to room temperature under H_2 to form the graphene-grown Cu foil. To transfer the graphene film, the graphene layer on the Cu foil was spin-coated with a poly(methyl methacrylate) (PMMA) support layer. The Cu film was removed using an aqueous etchant ($FeCl_3$), and the graphene/PMMA film was washed several times with deionized water. The graphene/PMMA film that floated was transferred onto a PS film and rinsed with acetic acid (99.9%) to remove PMMA.

Preparation of CNT film. First, sodium dodecyl sulfate (SDS, Aldrich, 99.9%) was dissolved in deionized water to prepare a surfactant solution. Multiwalled CNTs (Hanwha Chemical) were dispersed in the SDS solution to a concentration of 0.3 mg/ml. The prepared

solution was ultrasonicated for 1 h using a horn probe in an ice bath to prevent overheating and resultant degradation of the solution. The dispersed CNT solution was centrifuged at 5000 rpm for 10 min, and then the supernatant was collected to remove undispersed CNT bundles.

Preparation of graphene oxide. Graphene oxide (GO) was synthesized using the modified Hummer's method. First, graphite powder was added to a sulfuric acid solution (98%). Second, potassium permanganate was slowly added to the solution with vigorous stirring. The mixture was maintained at 35 °C for 4 h, and then it was diluted with deionized water in an ice bath to reduce overheating. Third, hydrogen peroxide was added to the diluted solution; here, the solution color changed from dark brown to yellow. The as-prepared GO solution was filtered, and the filtrate was washed several times with hydrochloric acid solution (10%) to remove the remaining inorganic impurities. The resultant GO was dispersed in deionized water to a concentration of 0.2 mg/ml for 30 min.

Fabrication of wrinkles. To form wrinkles of various materials on the polystyrene (PS) substrate, the target material was transferred onto PS by a method suitable for each material. The coated PS film was heated at a temperature greater than 135 °C for different periods to control the amount of strain. After strain relief, the coated PS film was rapidly cooled to room temperature. To calculate the strain of the PS film, the areas of a drawn box were measured, and the strain was determined using the equation $\varepsilon = (A_0 - A_f)/A_0$. The strain was controlled up to 0.80 by control of the heating time in the oven.

Characterization. Scanning electron microscopy (SEM; S-4800, Hitachi) images were recorded to observe the morphology of the wrinkled structure. Raman spectroscopy (Aramis, Horiba Jobin Yvon) was used to detect the peaks typical of various 2D materials, e.g., graphene, SnS_2, WS_2, and MoS_2. The spectrum was obtained by exposure of each film to a 514 nm laser

beam. Focused ion beam (FIB) SEM (Helios Nanolab 450 F1, FEI Company) was used to observe the cross sections of hierarchical MoS_2 and gold wrinkles in order to verify the threshold condition or inner structures. To compare the thickness and modulus of MoS_2, force versus distance curves were recorded by atomic force microscopy (XE-100, Park Systems) to calculate the modulus (**Figure S7**).

Electrochemical experiments. To verify the advantages of the wrinkles as a catalyst, the catalytic activity of MoS_2 wrinkles in hydrogen evolution was examined. The reaction was performed in a custom-made three-electrode electrochemical cell. MoS_2, platinum (Pt) wire, and a Ag/AgCl electrode were respectively used as the working, counter, and reference electrodes. To prepare MoS_2 wrinkles for the working electrode, MoS_2 wrinkles on a stainless-steel plate was prepared using a silver paste that was passivated by polymers. Electrolytes were prepared using 0.5 M H_2SO_4 Solution. Cyclic voltammetry curves were recorded between 0 V and −0.8 V versus reversible hydrogen electrode (RHE) at a scan rate of 5 mV/sec. For stability tests, the scan rate was 100 mV/sec.

Associated content

Supporting information

Details about experimental procedures. Figures S1−S26, reporting characterizations of materials and supporting experimental results of hierarchical wrinkle generation and catalysis. This material is available free of charge via the Internet at http://pubs.acs.org.

Acknowledgments

This research was supported by the National Research Foundation of Korea (NRF) grant funded by the Ministry of Science, ICT and future Planning, Korea (MSIP, NRF-2015R1A2A1A05001844). This work was supported by the Office of Naval Research (ONR N00014-17-1-2482).

References

(1) Pegan, J. D.; Ho, A. Y.; Bachman, M.; Khine, M. Flexible Shrink-Induced High Surface Area Electrodes for Electrochemiluminescent Sensing. *Lab. Chip* **2013,** *13*, 4205-4209.

(2) Wen, L.; Weaver, J. C.; Lauder, G. V. Biomimetic Shark Skin: Design, Fabrication and Hydrodynamic Function. *J. Exp. Biol.* **2014,** *217*, 1656-1666.

(3) Cao, Y.; Hutchinson, J. W. Wrinkling Phenomena in Neo-Hookean Film/Substrate Bilayers. *J. Appl. Mech.* **2012,** *79*, 031019.

(4) Lee, W. K.; Jung, W. B.; Nagel, S. R.; Odom, T. W. Stretchable Superhydrophobicity from Monolithic, Three-Dimensional Hierarchical Wrinkles. *Nano Lett.* **2016,** *16*, 3774-3779.

(5) Zhou, Q.; Kuhn, P. T.; Huisman, T.; Nieboer, E.; van Zwol, C.; van Kooten, T. G.; van Rijn, P. Directional Nanotopographic Gradients: a High-throughput Screening Platform for Cell Contact Guidance. *Sci. Rep.* **2015,** *5*, 16240.

(6) Aharoni, H.; Todorova, D. V.; Albarran, O.; Goehring, L.; Kamien, R. D.; Katifori, E. The Smectic Order of Wrinkles. *Nat. Commun.* **2017,** *8*, 15809.

(7) Zang, J.; Cao, C.; Feng, Y.; Liu, J.; Zhao, X. Stretchable and High-Performance Supercapacitors with Crumpled Graphene Papers. *Sci. Rep.* **2014,** *4*, 6492.

(8) Li, H.; Lu, C.; Ma, C.; Zhang, B. Wrinkled-graphene Wrapped Silicon Nanoparticles Synthesized Through Charged Colloidal Assembly for Enhanced Battery Performance. *Functional Materials Letters* **2014,** *07*, 1350067.

(9) Bae, H. J.; Bae, S.; Park, C.; Han, S.; Kim, J.; Kim, L. N.; Kim, K.; Song, S. H.; Park, W.; Kwon, S. Biomimetic Microfingerprints for Anti-Counterfeiting Strategies. *Adv. Mater.* **2015,** *27*, 2083-2089.

(10) Wang, L.; Castro, C. E.; Boyce, M. C. Growth Strain-Induced Wrinkled Membrane Morphology of White Blood Cells. *Soft Matter* **2011,** *7*, 11319.

(11) Zang, J.; Ryu, S.; Pugno, N.; Wang, Q.; Tu, Q.; Buehler, M. J.; Zhao, X. Multifunctionality and Control of The Crumpling and Unfolding of Large-area Graphene. *Nat. Mater.* **2013,** *12*, 321-325.

(12) Chae, S. H.; Yu, W. J.; Bae, J. J.; Duong, D. L.; Perello, D.; Jeong, H. Y.; Ta, Q. H.; Ly, T. H.; Vu, Q. A.; Yun, M.; Duan, X.; Lee, Y. H. Transferred Wrinkled Al2O3 for Highly Stretchable and Transparent Graphene-Carbon Nanotube Transistors. *Nat. Mater.* **2013,** *12*, 403-409.

(13) Sahabudeen, H.; Qi, H.; Glatz, B. A.; Tranca, D.; Dong, R.; Hou, Y.; Zhang, T.; Kuttner, C.; Lehnert, T.; Seifert, G.; Kaiser, U.; Fery, A.; Zheng, Z.; Feng, X. Wafer-sized Multifunctional Polyimine-based Two-Dimensional Conjugated Polymers with High Mechanical Stiffness. *Nat. Commun.* **2016,** *7*, 13461.

(14) Yu, S.; Sun, Y.; Ni, Y.; Zhang, X.; Zhou, H. Controlled Formation of Surface Patterns in Metal Films Deposited on Elasticity-Gradient PDMS Substrates. *ACS Appl. Mater. Interfaces* **2016,** *8*, 5706-5714.

(15) Chen, P. Y.; Sodhi, J.; Qiu, Y.; Valentin, T. M.; Steinberg, R. S.; Wang, Z.; Hurt, R. H.; Wong, I. Y. Multiscale Graphene Topographies Programmed by Sequential Mechanical Deformation. *Adv. Mater.* **2016,** *28*, 3564-3571.

(16) Yoo, P. J.; Lee, H. H. Evolution of a Stress-Driven Pattern in thin bilayer films: spinodal wrinkling. *Phys. Rev. Lett.* **2003,** *91*, 154502.

(17) Moon, M.-W.; Lee, S. H.; Sun, J.-Y.; Oh, K. H.; Vaziri, A.; Hutchinson, J. W. Wrinkled Hard Skins on Polymers Created by Focused Ion Beam. *Proc. Natl. Acad. Sci. U. S. A.* **2006,** *104*, 1130-1133.

(18) Kim, P.; Abkarian, M.; Stone, H. A. Hierarchical Folding of Elastic Membranes under Biaxial Compressive Stress. *Nat. Mater.* **2011,** *10*, 952-957.

(19) Efimenko, K.; Rackaitis, M.; Manias, E.; Vaziri, A.; Mahadevan, L.; Genzer, J. Nested Self-Similar Wrinkling Patterns in Skins. *Nat. Mater.* **2005,** *4*, 293-297.

(20) Lee, W. K.; Engel, C. J.; Huntington, M. D.; Hu, J.; Odom, T. W. Controlled Three-Dimensional Hierarchical Structuring by Memory-Based, Sequential Wrinkling. *Nano Lett.* **2015,** *15*, 5624-5629.

(21) Chen, P. Y.; Liu, M.; Valentin, T. M.; Wang, Z.; Spitz Steinberg, R.; Sodhi, J.; Wong, I. Y.; Hurt, R. H. Hierarchical Metal Oxide Topographies Replicated from Highly Textured Graphene Oxide by Intercalation Templating. *ACS Nano* **2016,** *10*, 10869-10879.

(22) Huntington, M. D.; Engel, C. J.; Hryn, A. J.; Odom, T. W. Polymer Nanowrinkles with Continuously Tunable Wavelengths. *ACS Appl. Mater. Interfaces* **2013,** *5*, 6438-6442.

(23) Huntington, M. D.; Engel, C. J.; Odom, T. W. Controlling The Orientation of Nanowrinkles and Nanofolds by Patterning Strain in a Thin Skin Layer on a Polymer Substrate. *Angew. Chem. Int. Ed. Engl.* **2014,** *53*, 8117-8121.

(24) Greco, F.; Bellacicca, A.; Gemmi, M.; Cappello, V.; Mattoli, V.; Milani, P. Conducting Shrinkable Nanocomposite Based on Au-Nanoparticle Implanted Plastic Sheet: Tunable Thermally Induced Surface Wrinkling. *ACS Appl. Mater. Interfaces* **2015,** *7*, 7060-7065.

(25) Chen, A.; Lieu, D. K.; Freschauf, L.; Lew, V.; Sharma, H.; Wang, J.; Nguyen, D.; Karakikes, I.; Hajjar, R. J.; Gopinathan, A.; Botvinick, E.; Fowlkes, C. C.; Li, R. A.; Khine, M. Shrink-Film Configurable Multiscale Wrinkles for Functional Alignment of Human Embryonic Stem Cells and Their Cardiac Derivatives. *Adv. Mater.* **2011,** *23*, 5785-5791.

(26) Lee, W. K.; Kang, J.; Chen, K. S.; Engel, C. J.; Jung, W. B.; Rhee, D.; Hersam, M. C.; Odom, T. W. Multiscale, Hierarchical Patterning of Graphene by Conformal Wrinkling. *Nano Lett.* **2016,** *16*, 7121-7127.

(27) Kong, D.; Wang, H.; Cha, J. J.; Pasta, M.; Koski, K. J.; Yao, J.; Cui, Y. Synthesis of MoS2 and MoSe2 Films with Vertically Aligned Layers. *Nano Lett.* **2013,** *13*, 1341-1347.

(28) Jiao, L.; Fan, B.; Xian, X.; Wu, Z.; Zhang, J.; Liu, Z. Creation of Nanostructures with Poly(methyl methacrylate)-Mediated Nanotransfer Printing *J. Am. Chem. Soc.* **2008,** *130*, 12612-12613.

(29) Birleanu, C.; Pustan, M.; Merie, V.; Müller, R.; Voicu, R.; Baracu, A.; Craciun, S. Temperature Effect on The Mechanical Properties of Gold Nano Films with Different Thickness. *IOP Conference Series: Materials Science and Engineering* **2016,** *147*, 012021.

(30) Li, X.; Colombo, L.; Ruoff, R. S. Synthesis of Graphene Films on Copper Foils by Chemical Vapor Deposition. *Adv. Mater.* **2016,** *28*, 6247-6252.

(31) Jiang, J.-W.; Wang, J.-S.; Li, B. Young's Modulus of Graphene: A Molecular Dynamics Study. *Phys. Rev. B* **2009,** *80*, 113405.

(32) Ni, Z. H.; Wang, H. M.; Kasim, J.; Fan, H. M.; Yu, T.; Wu, Y. H.; Feng, Y. P.; Shen, Z. X. Graphene Thickness Determination Using Reflection and Contrast Spectroscopy. *Nano Lett.* **007,** *7*, 2758-2763.

(33) Marcano, D. C.; Kosynkin, D. V.; Berlin, J. M.; Sinitskii, A.; Sun, Z.; Slesarev, A.; Alemany, L. B.; Lu, W.; Tour, J. M. Improved Synthesis of Graphene Oxide. *ACS Nano* **2010,** *4*, 4806-4814.

(34) Suk, J. W.; Piner, R. D.; An, J.; Ruoff, R. S. Mechanical Properties of Monolayer Graphene Oxide. *ACS Nano* **2010,** *4*, 6557-6564.

(35) Elı´as, A. L.; pez, N. s. P.-L.; Castro-Beltra´n, A. s.; Berkdemir, A.; Lv, R.; Feng, S.; Long, A. D.; Hayashi, T.; Kim, Y. A.; Endo, M.; rrez, H. R. G.; Pradhan, N. R.; Balicas, L.; Mallouk, T. E.; Lo´pez-Urı´as, F.; Terrones, H.; Terrones, M. Controlled Synthesis and Transfer of Large-Area WS2 Sheets: From Single Layer to Few Layers. *ACS Nano* **2013,** *7*, 5235-5242.

(36) Huang, Y.; Deng, H. X.; Xu, K.; Wang, Z. X.; Wang, Q. S.; Wang, F. M.; Wang, F.; Zhan, X. Y.; Li, S. S.; Luo, J. W.; He, J. Highly Sensitive and Fast Phototransistor Based on Large Size CVD-Grown SnS2 Nanosheets. *Nanoscale* **2015,** *7*, 14093-14099.

(37) Geng, X.; Sun, W.; Wu, W.; Chen, B.; Al-Hilo, A.; Benamara, M.; Zhu, H.; Watanabe, F.; Cui, J.; Chen, T. P. Pure and Stable Metallic Phase Molybdenum Disulfide Nanosheets for Hydrogen Evolution Reaction. *Nat. Commun.* **2016,** *7*, 10672.

(38) Duan, W. H.; Wang, Q.; Collins, F. Dispersion of Carbon Nanotubes with SDS Surfactants: A Study from a Binding Energy Perspective. *Chemical Science* **2011,** *2*, 1407.

(39) Scarratt, L. R.; Hoatson, B. S.; Wood, E. S.; Hawkett, B. S.; Neto, C. Durable Superhydrophobic Surfaces via Spontaneous Wrinkling of Teflon AF. *ACS Appl. Mater. Interfaces* **2016,** *8*, 6743-6750.

(40) Glatz, B. A.; Tebbe, M.; Kaoui, B.; Aichele, R.; Kuttner, C.; Schedl, A. E.; Schmidt, H. W.; Zimmermann, W.; Fery, A. Hierarchical Line-Defect Patterns in Wrinkled Surfaces. *Soft Matter* **2015,** *11*, 3332-3339.

(41) Voiry, D.; Salehi, M.; Silva, R.; Fujita, T.; Chen, M.; Asefa, T.; Shenoy, V. B.; Eda, G.; Chhowalla, M. Conducting MoS2 Nanosheets as Catalysts for Hydrogen Evolution Reaction. *Nano Lett.* **2013,** *13*, 6222-6227.

(42) Jaramillo, T. F.; Jørgensen, K. P.; Bonde, J.; Nielsen, J. H.; Horch, S.; Chorkendorff, I. Identification of Active Edge Sites for Electrochemical H2 Evolution from MoS2 Nanocatalysts. *Science* **2007,** *317*, 100-102.

(43) Li, G.; Zhang, D.; Qiao, Q.; Yu, Y.; Peterson, D.; Zafar, A.; Kumar, R.; Curtarolo, S.; Hunte, F.; Shannon, S.; Zhu, Y.; Yang, W.; Cao, L. All The Catalytic Active Sites of MoS2 for Hydrogen Evolution. *J. Am. Chem. Soc.* **2016,** *138*, 16632-16638.

(44) Li, Y.; Wang, H.; Xie, L.; Liang, Y.; Hong, G.; Dai, H. MoS2 Nanoparticles Grown on Graphene: An Advanced Catalyst for The Hydrogen Evolution Reaction. *J. Am. Chem. Soc.* **2011,** *133*, 7296-7299.

(45) Ma, L.; Ting, L. R. L.; Molinari, V.; Giordano, C.; Yeo, B. S. Efficient Hydrogen Evolution Reaction Catalyzed by Molybdenum Carbide and Molybdenum Nitride Nanocatalysts Synthesized via The Urea Glass Route. *J. Mater. Chem. A* **2015,** *3*, 8361-8368.

(46) Lu, Z.; Zhu, W.; Yu, X.; Zhang, H.; Li, Y.; Sun, X.; Wang, X.; Wang, H.; Wang, J.; Luo, J.; Lei, X.; Jiang, L. Ultrahigh Hydrogen Evolution Performance of Under-Water "Superaerophobic" MoS2 Nanostructured Electrodes. *Adv. Mater.* **2014,** *26*, 2683-2687.

(47) Kim, J. Y.; Lim, J.; Jin, H. M.; Kim, B. H.; Jeong, S. J.; Choi, D. S.; Li, D. J.; Kim, S. O. 3D Tailored Crumpling of Block-Copolymer Lithography on Chemically Modified Graphene. *Adv. Mater.* **2016,** *28*, 1591-1596.

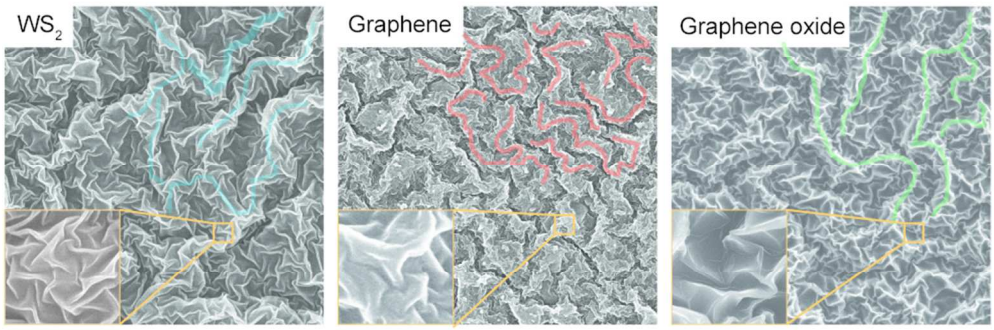

ToC

84x36mm (300 x 300 DPI)

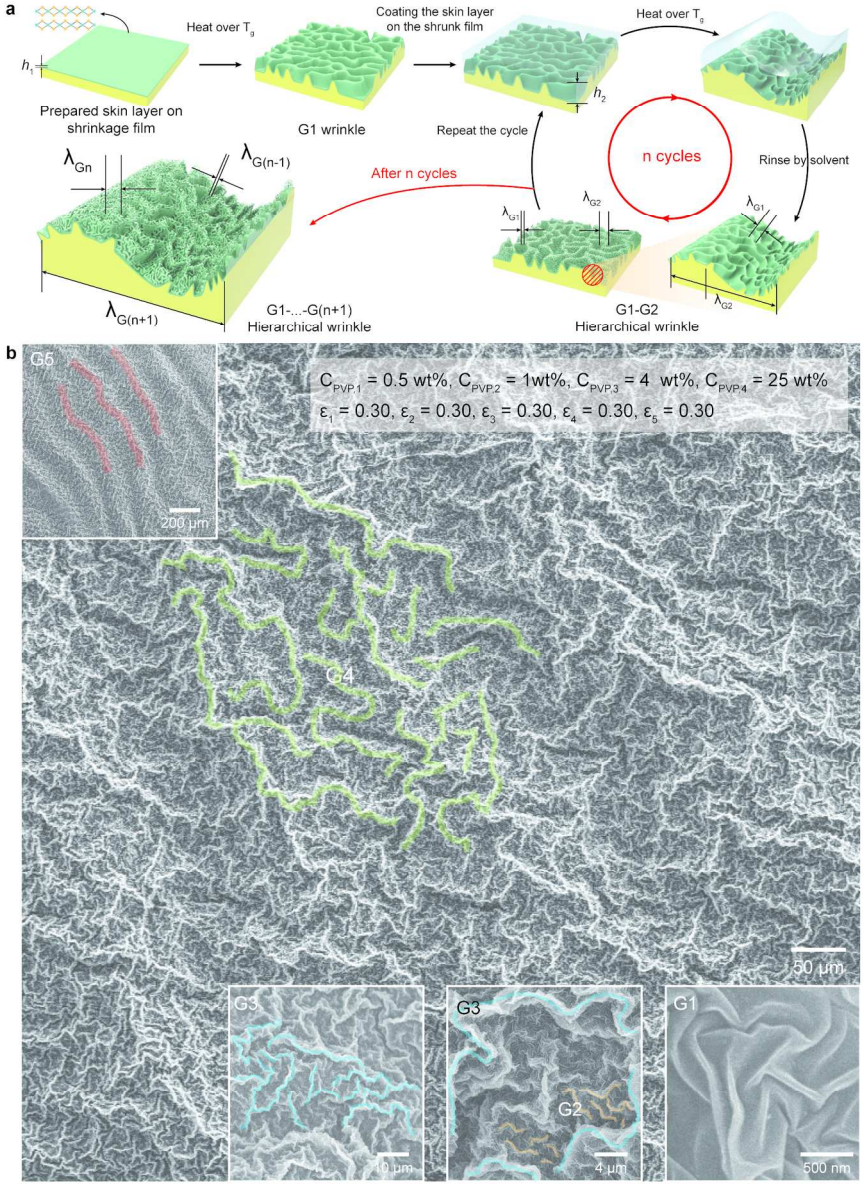

Figure 1. Schematic for the fabrication of hierarchical wrinkles. (a) Hierarchical wrinkling process (b) Hierarchical MoS2 wrinkle including G1–G5 after four cycles of hierarchical wrinkling.

160x207mm (300 x 300 DPI)

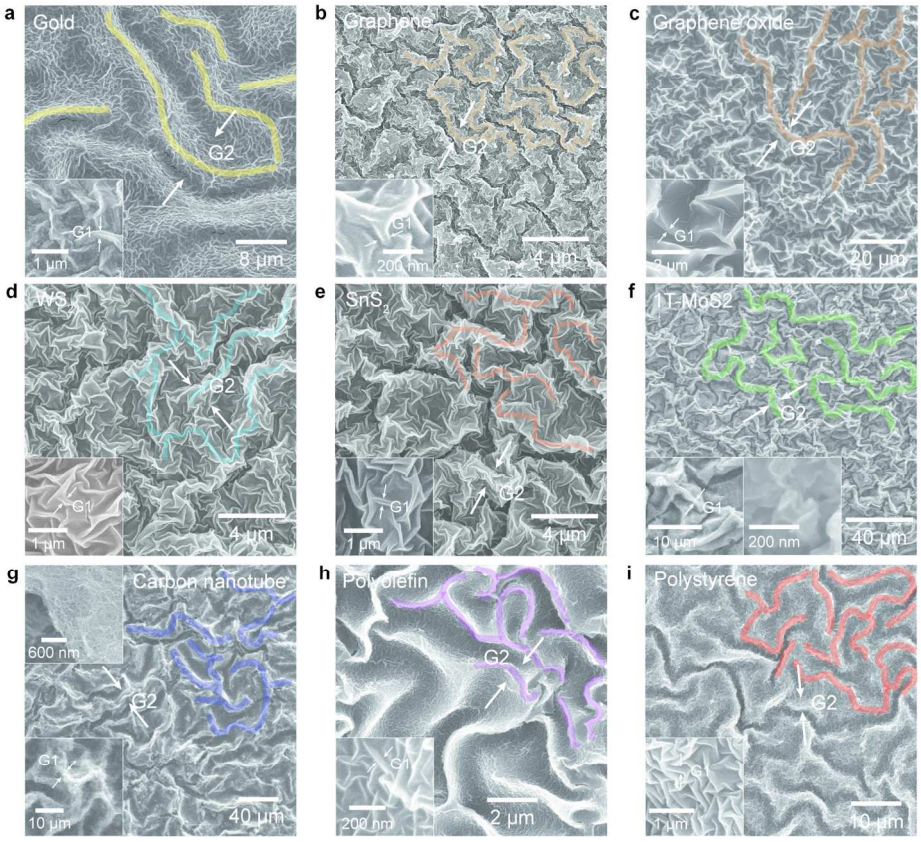

Figure 2. Hierarchical wrinkles obtained by using various materials. (a) Gold, (b) Graphene, (c) graphene oxide, (d) tungsten disulfide (WS2), (e) tin disulfide (SnS2), (f) 1T-MoS2, (g) carbon nanotubes, (h) polyolefin, and (i) polystyrene. Inset images show high-magnification SEM images002E

160x138mm (300 x 300 DPI)

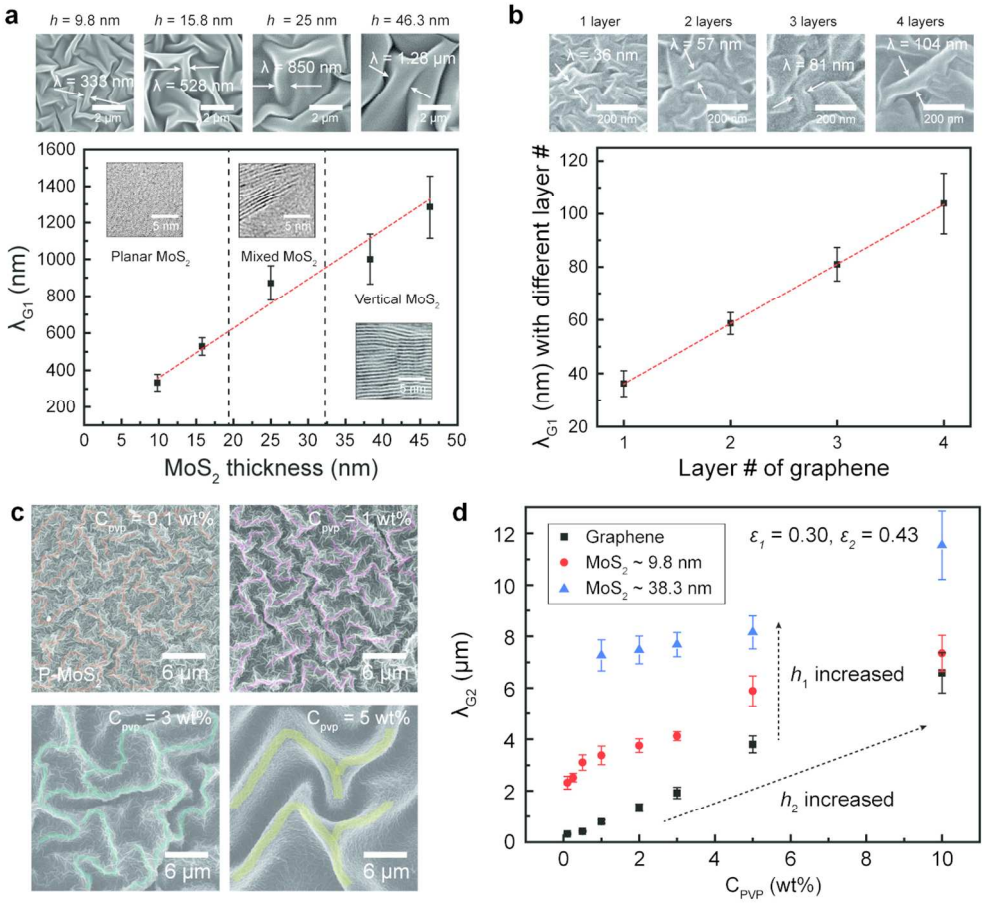

Figure 3. Tunable wavelength of hierarchical MoS2 and graphene wrinkle. (a) Wavelength is proportional to the thickness of MoS2, and each film exhibits different atomic structures. (b) Increase in the graphene layer for controlling λG1: (c) Hierarchical 9.8 nm thick MoS2 wrinkle with different CPVP, which changes λG2. (d) CPVP versus λG2. λG2 is proportional to CPVP and skin thickness (h1).

119x109mm (300 x 300 DPI)

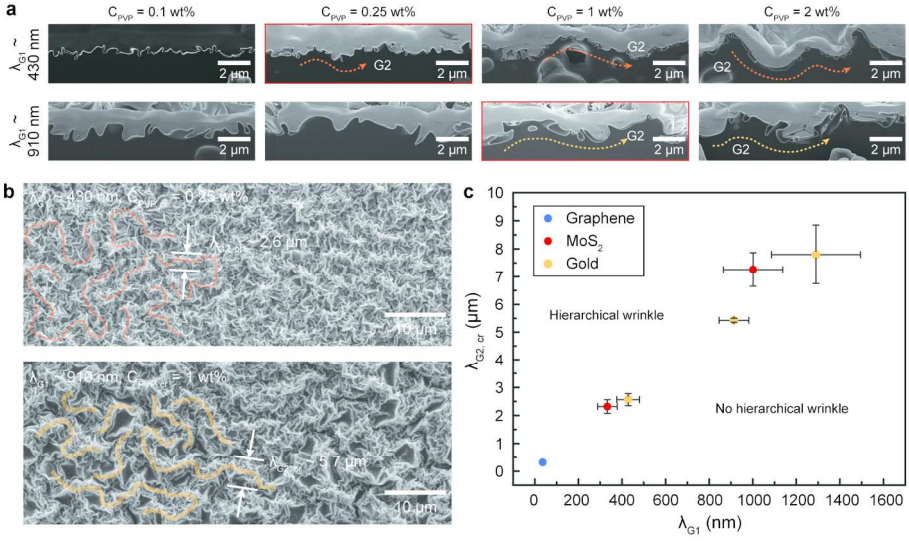

Figure 4. Critical conditions for the formation of hierarchical wrinkles. (a) FIB-SEM images of hierarchical Au wrinkles with λG1 and CPVP from 0.1 wt% to 2 wt%. (b) SEM images at CPVP, cr. (c) λG1 vs. λG2, cr plots for the materials with MoS2, graphene, and gold.

160x87mm (300 x 300 DPI)

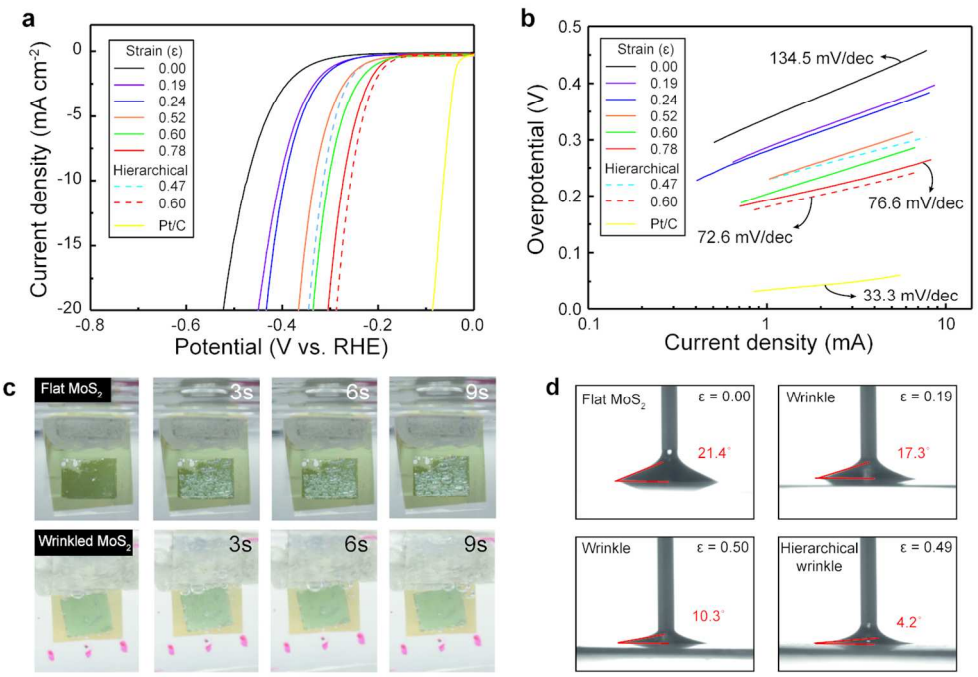

Figure 5. Effect of wrinkles on the HER activity of MoS2. (a) LSV curves of primary wrinkles, hierarchical wrinkles (dashed line) at various strain values, and the Pt/C reference. (b) Corresponding Tafel plots of the LSV curves. (c) Photograph of the surfaces of flat and wrinkled MoS2 surfaces producing hydrogen gas. (d) Receding contact angles on flat MoS2 and on various wrinkles.

124x85mm (300 x 300 DPI)